Weighted Time Warping T-Wave Analysis Robust to Delineation Errors: Clinical Implications

Flavio Palmieri[1,2,3], Pedro Gomis[1,2], José Esteban Ruiz[4], Dina Ferreira[3], Esther Pueyo[2,5], Juan Pablo Martínez[2,5], Pablo Laguna[2,5] and Julia Ramírez[6]

[1] Centre de Recerca en Enginyeria Biomèdica, Universitat Politècnica de Catalunya, Barcelona, Spain
[2] CIBER en Bioingeniería, Biomateriales y Nanomedicina (CIBER-BBN), Zaragoza, Spain
[3] Laboratorios Rubio, Castellbisbal, Barcelona, Spain
[4] Nephrology Department, Hospital Clínico Universitario Lozano Blesa, Zaragoza, Spain
[5] BSICoS Group, I3A, IIS Aragón, Universidad de Zaragoza, Zaragoza, Spain
[6] William Harvey Research Institute, Queen Mary University of London, London, United Kingdom

Abstract

T-wave (TW) morphology has been extensively investigated to develop specific risk prediction markers like d_w quantifying the level of warping needed to temporally align a TW respect to a reference one. However, TW boundaries delineation errors may jeopardise d_w diagnostic power. Hence, we proposed two TW-based weighting function (WFs) obtained from (i) the reference TW ($\mathcal{T}$), and (ii) the absolute value of its first-derivative ($\mathcal{D}$). We, first, simulated TW boundaries delineation errors by shortening and widening two TWs with morphological variability. We, then, used the variation ratio ($\mathcal{R}$) to compare d_w derived applying the two WFs with that obtained in the control case (no weighting, $\mathcal{C}$). Next, we compared the ability of d_w, with and without WFs, in monitoring blood potassium concentration changes ($\Delta[K^+]$) by means of the Pearson's correlation (r) in 29 48-hour Holter recordings from hemodyalisis (HD) patients. The simulations showed that $\mathcal{R}$ values for the two studied TWs, respectively, were 0.17 and 0.19 for $\mathcal{C}$, 0.05 and 0.08 for $\mathcal{T}$ and 0.07 and 0.10 for $\mathcal{D}$. However, similar r median [interquartile range] values were found for $\mathcal{C}$ (0.90 [0.27]), $\mathcal{T}$ (0.90 [0.25]) and $\mathcal{D}$ (0.90 [0.29]) in HD scenario. Thus, using WFs to compute d_w reduces the effects of TW boundaries delineation errors, but no improvements in $\Delta[K^+]$ monitoring in HD patients were observed. WFs impact on d_w risk prediction power remains to be studied.

1. Introduction

The T-wave (TW) morphology on the electrocardiogram (ECG) has been extensively investigated in an attempt to identify sensitive and specific markers of risk in different scenarios, such as sudden cardiac death (SCD) risk stratification [1]. In particular, the TW morphology marker d_w, which quantifies the level of warping needed to temporally align a studied TW morphology with respect to a reference TW morphology [1], has demonstrated a good correlation with dispersion of ventricular repolarization and arrhythmic risk [2]. Automatic location of TW boundaries is a necessary step in the calculation of d_w, but it is highly susceptible to noise and misplacement, especially in cases with low TW amplitude and morphological variability [3]. Errors in locating TW boundaries may greatly affect the robustness and sensitivity of d_w, thus potentially impacting its risk stratification value. We hypothesised that adding a weighting step in the calculation of d_w would reduce the effect of errors in locating the TW boundaries.

We proposed two weighting functions (WFs): (i) the reference TW itself, $\mathcal{W}_{\mathcal{T}}(t)$, and (ii) the absolute value of its first-time derivative, $\mathcal{W}_{\mathcal{D}}(t)$. We, then, tested the robustness of the resulting d_w markers against simulated TW boundary errors, and their ability to monitor blood potassium concentration ($[K^+]$) changes during a hemodyalisis (HD) treatment, and compared their performance respect to the control no weighting case $\mathcal{C}$, $\mathcal{W}_{\mathcal{C}}(t) = 1$.

2. Materials

ECGs used in the simulation of boundary errors: A reference TW was extracted from a noise-free heartbeat, sampled at 1 kHz, recorded at supine position from a healthy subject [4].

Hemodyalisis dataset: Twenty-nine standard 12-lead, 48-hour ECG Holter (sampled at 1 kHz) from end-stage renal disease patients undergoing HD (ESRD-HD) at Hospital Clínico Universitario Lozano Blesa (Zaragoza, Spain) [5], were analysed. For each patient, five $[K^+]$ measure-

 ISSN: 2325-887X DOI: 10.22489/CinC.2021.100

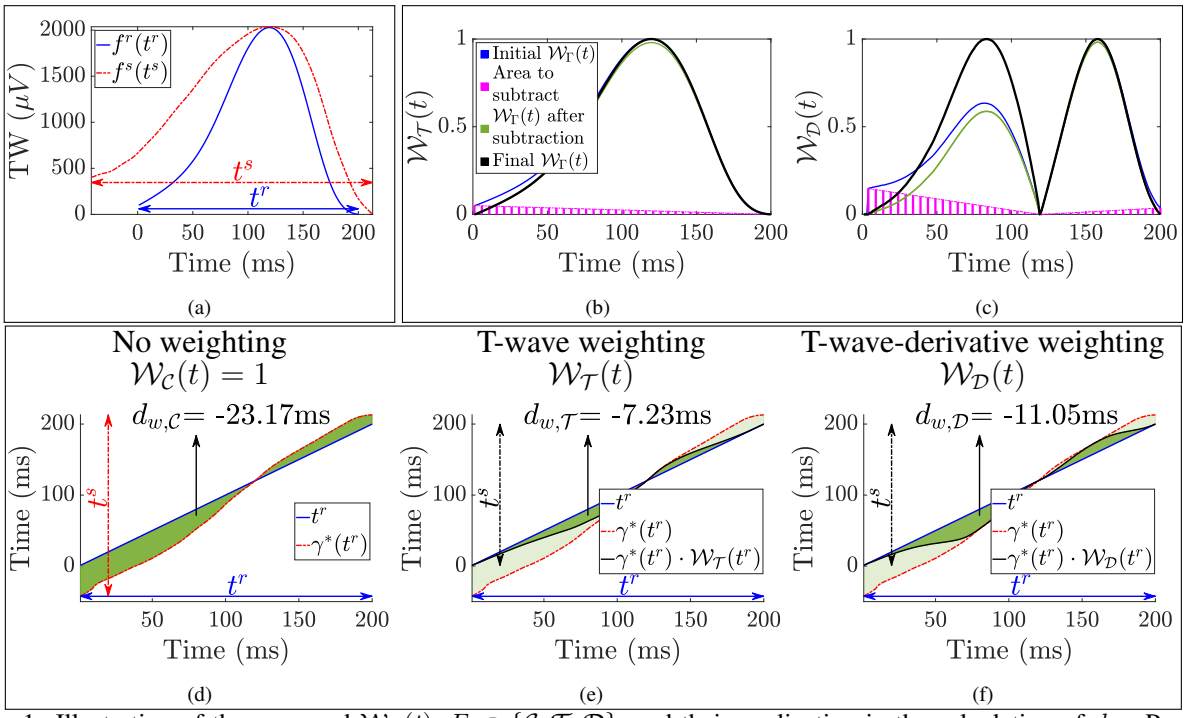

Figure 1: Illustration of the proposed $\mathcal{W}_\Gamma(t)$, $\Gamma \in \{\mathcal{C}, \mathcal{T}, \mathcal{D}\}$, and their application in the calculation of d_w. Panel (a) shows the reference and studied TW (blue and red, respectively). Panels (b) and (c) show the process to derive both $\mathcal{W}_\mathcal{T}(t)$ and $\mathcal{W}_\mathcal{D}(t)$, respectively, as detailed in section 3. Panel (d) shows the calculation of the control $d_{w,\mathcal{C}}$ (dark green area under $\gamma^*(\boldsymbol{t}^r)$), while panels (e) and (f) show the calculation of $d_{w,\mathcal{T}}$ and $d_{w,\mathcal{D}}$, estimated as $\gamma^*(\boldsymbol{t}^r) \cdot \mathcal{W}_\mathcal{T}(t^r)$ and $\gamma^*(\boldsymbol{t}^r) \cdot \mathcal{W}_\mathcal{D}(t^r)$, respectively, obtaining the updated dark green areas.

ments were taken: one at the HD onset (h_0), three every following hour (h_1, h_2 and h_3) and one at the HD end (h_4).

3. Methods

Periodic component analysis (πC) is an eigenvalue decomposition technique whose aim is to extract the most periodic sources of the signal. In this study, πC was spatially applied to maximize the TW beat-to-beat periodic components on the first transformed lead as in [6].

Weighting function and d_w computation: Let $\boldsymbol{f}^r(\boldsymbol{t}^r)$ be a reference TW and $\boldsymbol{f}^s(\boldsymbol{t}^s)$ the studied TW (Fig. 1a in blue and red respectively), with $\boldsymbol{t}^r = [t^r(1), ..., t^r(N_r)]^\top$ and $\boldsymbol{t}^s = [t^s(1), ..., t^s(N_s)]^\top$ their time duration with N_r and N_s the total length of $\boldsymbol{t}^r$ and $\boldsymbol{t}^s$, respectively.

The first proposed $\mathcal{W}_\mathcal{T}(t)$ was taken as the reference TW itself by normalizing $\boldsymbol{f}^r(\boldsymbol{t}^r)$ by its maximum value (Fig. 1b, blue TW). Then, the residual area under the TW, defined by linear extreme connection (Fig. 1b, magenta) was subtracted, obtaining the green TW (Fig. 1b), which was normalized further by its maximum value, resulting in the final $\mathcal{W}_\mathcal{T}(\boldsymbol{t}^r)$ (Fig. 1b, black). In doing so, there is no weighting applied to TW extremes, hence reducing the effect of boundary delineation errors.

To compute the second WF, $\mathcal{W}_\mathcal{D}(\boldsymbol{t}^r)$, we divided the absolute value of the reference TW $\boldsymbol{f}^r(\boldsymbol{t}^r)$ first-time derivative in two halves, being the middle zero value (corresponding to the $\boldsymbol{f}^r(\boldsymbol{t}^r)$ peak) the splitting point. Then, the same procedure previously described was individually applied to each half. Next, the two parts were linked, obtaining $\mathcal{W}_\mathcal{D}(\boldsymbol{t}^r)$ (Fig. 1c).

The optimal warping function $\gamma^*(\boldsymbol{t}^r)$ relating $\boldsymbol{f}^r(\boldsymbol{t}^r)$ and $\boldsymbol{f}^s(\boldsymbol{t}^s)$ ($\gamma^*(\boldsymbol{t}^r)$, with no weighting, Fig. 1d dashed red line) [1] was multiplied by both $\mathcal{W}_\mathcal{T}(\boldsymbol{t}^r)$ ($\gamma^*(\boldsymbol{t}^r) \cdot \mathcal{W}_\mathcal{T}(t^r)$, Fig. 1e black solid line) and $\mathcal{W}_\mathcal{D}(\boldsymbol{t}^r)$ ($\gamma^*(\boldsymbol{t}^r) \cdot \mathcal{W}_\mathcal{D}(t^r)$, Fig. 1f black solid line), respectively. The total warping information (dark green area) was quantified by d_w [5]:

$$d_w = \left(\frac{s_d}{|s_d|}\right) \frac{1}{N_r} \sum_{n=1}^{N_r} |\gamma^*\left(t^r\left(n\right)\right) - t^r\left(n\right)| \quad (1)$$

$$s_d = \sum_{n \in N_r^u} \left(\gamma^*\left(t^r\left(n\right)\right) - t^r\left(n\right)\right) + \sum_{n \notin N_r^u} \left(t^r\left(n\right) - \gamma^*\left(t^r\left(n\right)\right)\right) \quad (2)$$

with N_r^u being the set of up-slope samples. A positive sign means that the $\boldsymbol{f}^s(\boldsymbol{t}^s)$ has to be widened to fit the $\boldsymbol{f}^r(\boldsymbol{t}^r)$, and vice-versa for a negative sign.

Simulation of boundary errors: From the $\boldsymbol{f}^r(\boldsymbol{t}^r)$ in Fig. 2a, two modulated TWs, $\boldsymbol{f}^s(\boldsymbol{t}^s)$ with $s \in \{1, 2\}$ counting for the cases in Fig. 2b and 2c, were obtained

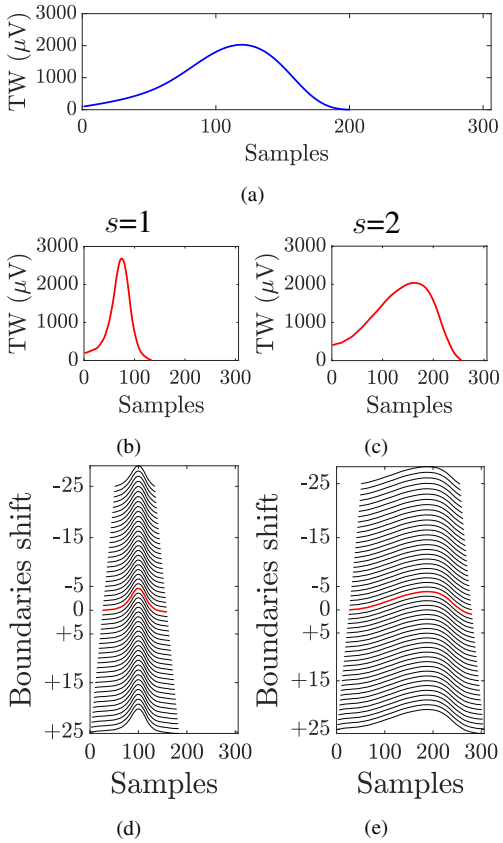

Figure 2: Simulated TW modulation and boundary shift. Panel (a) shows the reference TW from which the two modulated TWs, $s \in \{1, 2\}$, are obtained (panels (b) and (c), respectively) after adding linear and nonlinear time and amplitude variability. Panels (d) and (e) show the resulting TWs after simulating shifts in the boundaries for both modulated TWs (in red).

by first generating nonlinear TW amplitude variability as:

$$\boldsymbol{f}^s_{\text{NL}}(\boldsymbol{t}^r) = \boldsymbol{f}^r(\boldsymbol{t}^r) + c(s) \cdot \sin\left(2\pi \frac{1}{4N_r} \boldsymbol{t}^r\right) \quad (3)$$

where $c(1)$=150 and $c(2)$=-150. Then, linear TW amplitude variability was included as $\boldsymbol{f}^s(\boldsymbol{t}^r) = \boldsymbol{f}^s_{\text{NL}}(\boldsymbol{t}^r) \cdot b(s)$, being $b(1)$=1.15 and $b(2)$=0.85. Next, the linear TW duration variability was generated as $\boldsymbol{t}^s_l = \gamma_s(\boldsymbol{t}^r)$, where $\gamma_s(\boldsymbol{t}^r)$ up and downsamples $\boldsymbol{t}^r$ based on sampling factor, $k(1)$=0.7 and $k(2)$=1.3. Finally, the linear plus non linear TW duration variability was generated by:

$$\boldsymbol{t}^s = \boldsymbol{t}^s_l + d(s)\frac{N_r}{N_s} \cdot \sin\left(2\pi \frac{1}{N_r} \boldsymbol{t}^s_l\right) \quad (4)$$

where $d(1)$=-15 and $d(2)$=15 and N_s is the $\boldsymbol{t}^s_l$ duration. The whole TW duration and amplitude variability was:

$$\boldsymbol{f}^s(\boldsymbol{t}^s) = \boldsymbol{f}^s\left(\gamma_s(\boldsymbol{t}^r) + d(s)\frac{N_r}{N_s} \cdot \sin\left(2\pi \frac{1}{N_r}\gamma_s(\boldsymbol{t}^r)\right)\right) \quad (5)$$

Later, for both cases $\boldsymbol{f}^s(\boldsymbol{t}^s)$ and $\boldsymbol{f}^r(\boldsymbol{t}^r)$, we simulated T-wave boundary delineation errors as shifts in the TW onset and end points by progressively removing (adding) n samples, starting by n=1 sample (1 ms), up to n=25, as shown in Fig. 2d and Fig. 2e (black TWs), resulting in TW boundaries variability, $\sigma = 14.9$ ms, within the TW end measurements tolerance reported by manual experts [7]. Next, d_w was computed by time warping each boundary-shifted TW and the reference TW (Fig. 2a) with and without applying the two WFs. Thus, for both cases, $s \in \{1, 2\}$ (Fig. 2d and 2e, respectively) and weightings, $\Gamma \in \{\mathcal{C}, \mathcal{T}, \mathcal{D}\}$, three $d^s_{w,\Gamma}(n)$, $n \in \{1, \cdots, 25\}$, series were extracted. Finally, a variation ratio ($\mathcal{R}$) was computed for each case as:

$$\mathcal{R}^s_\Gamma = \frac{\sigma(d^s_{w,\Gamma}(n))}{|d^s_{w,\Gamma}(n=0)|}, \quad (6)$$

where $d^s_{w,\Gamma}(n$=0) is the marker value computed when no shift is performed (Fig. 2d and 2e, in red), and $\sigma(d^s_{w,\Gamma}(n))$ is the standard deviation of the series.

Hemodyalisis dataset: ECGs were band-pass filtered (40 Hz high cut-off) to remove muscular and power-line noise and high-pass filtered (0.5 Hz low cut-off) to attenuate baseline wander. QRS complexes were detected and delineated in each lead using a wavelet-based delineation method [8]. Then, a πC transformation matrix was estimated from a excerpt of the signal and applied to the 8 independent leads [6]. Finally, for each patient, all TWs in the first πC were delineated [8] and the warping analysis was performed as in [5]. Five mean warped TWs (MWTW) were extracted at hours h_i $i \in \{0, 1, 2, 3, 4\}$ by averaging the TWs within 2-min wide window centered in coincidence of each the $[K^+]$ values [5]. The MWTW and $[K^+]$ corresponding to h_4 were, respectively, the reference for the time warping and for the relative [K$^+$] variations ($\Delta[K^+]$) evaluation; while the MWTWs and $[K^+]$ values at hours h_0, h_1, h_2 and h_3 were, respectively, the four studied MWTWs (for time warping analysis) and $[K^+]$ concentrations for $\Delta[K^+](i) = [K^+]_{h_i} - [K^+]_{h_4}$ computation being $[K^+]_{h_i}$ the concentration at the i-th hour. For each patient, Pearson's (r) correlation between the five $\Delta[K^+]$ and each corresponding value of d_w, derived with ($d_{w,\mathcal{T}}$ and $d_{w,\mathcal{D}}$) and without ($d_{w,\mathcal{C}}$) applying the WFs, was evaluated.

4. Results and Discussion

Effects of Weighting: A clear reduction of the d_w value (dark green area) can be observed by comparing Fig. 1d, with respect to both Fig. 1e and 1f, particularly at the boundary regions (light green area) as a consequence of the weighting procedure. The $\mathcal{W}_\mathcal{D}(t)$ proposal was introduced since the warping function typically gets close to zero values at the TW peak (see Fig. 1d) and then we hypothesised the derivative would emphasise the centres of

the two halves in Fig. 1d, being the richest parts in terms of electrophysiological information [9]. This resulted in a warping function, Fig. 1f, where the centre of the two halves was emphasised, while the extremes, more prone to delineation error, were attenuated.

Simulation of boundary errors: Table 1 shows the $\mathcal{R}$ values for the two simulated cases demonstrating that the relative dispersion with respect to the reference (when no shift is performed), is significantly reduced when the WFs are applied, thus confirming their hypothesised ability to minimize the effects of TW boundaries delineation errors. Moreover, $\mathcal{R}_{\mathcal{T}}$ values for both $s \in \{1, 2\}$ are smaller than those from $\mathcal{R}_{\mathcal{D}}$, suggesting a slightly better performance of $\mathcal{W}_{\mathcal{T}}(t)$ with respect to $\mathcal{W}_{\mathcal{D}}(t)$. However, results are still very similar to draw strong conclusions about which is the most suitable WF for d_w computation.

Table 1: Variation ratio $\mathcal{R}^s_{\Gamma}$; $s \in \{1, 2\}$; $\Gamma \in \{\mathcal{C}, \mathcal{T}, \mathcal{D}\}$.

s	$\mathcal{R}_{\mathcal{C}}$	$\mathcal{R}_{\mathcal{T}}$	$\mathcal{R}_{\mathcal{D}}$
1	0.17	0.05	0.07
2	0.19	0.08	0.10

Hemodyalisis dataset: Fig. 3 shows $\Delta[K^+]$ and $d_{w,\Gamma}$ distributions during the HD in the study population. All markers follow a similar magnitude decreasing trend, regardless of whether or not a WF was applied, but the variation range clearly decreases with the use of weighting, as shown in Fig. 3. Similar r median [interquartile range] values were found for $d_{w,\mathcal{C}}$ (0.90 [0.27]), $d_{w,\mathcal{T}}$ (0.90 [0.25]) and $d_{w,\mathcal{D}}$ (0.90 [0.29]). This would suggest that the effects of TW boundaries delineation errors were small enough not to affect the d_w ability of [K^+] tracking, possibly because those errors may have been already reduced by the averaging performed to compute the MWTWs [5].

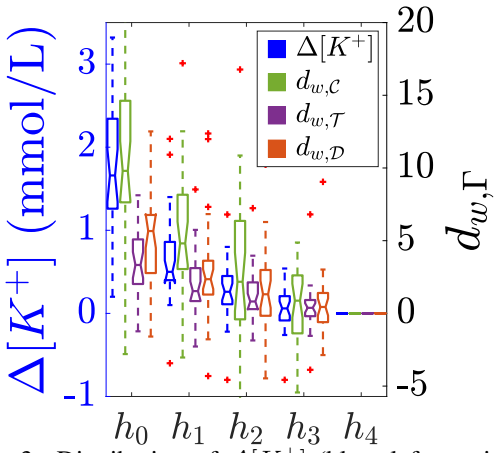

Figure 3: Distribution of $\Delta[K^+]$ (blue, left y-axis) and $d_{w,\Gamma}$, $\Gamma \in \{\mathcal{C}, \mathcal{T}, \mathcal{D}\}$ (green, purple and orange, respectively, right y-axis), during the HD session. Outliers are indicated in red.

Limitations and future works: While the simulation test proved the usefulness of the WFs in reducing the effects of TW delineation error on warping, it did not improve [K^+] monitoring in ESRD-HD patients. New studies on ECGs where the influence of TW morphology changes are tiny, such as in SCD prediction, will determine the advantages of using the proposed weighting method.

5. Conclusions

These results confirm the ability of WFs in reducing the undesired effects of TW boundaries delineation errors in d_w computation but the improvements in [K^+] monitoring are negligible. WFs impact on scenarios evaluating the risk stratification value of d_w remains to be evaluated.

Acknowledgements

This work was funded by Products & Technology S.L. (Spain), and by AGAUR (Spain) grant DI001-2018 and CIBER-BBN ref: "*DEKOALE*". The work was also supported by project PID2019-104881RB-I00, and PID2019-105674RB-I00 funded by Spanish Ministry of Science and Innovation (MICINN) and FEDER, by Gobierno de Aragón (Reference Group (BSICoS) T39-20R) co-funded by FEDER 2014-2020 "*Building Europe from Aragón*", and by European Research Council (ERC) through project ERC-StG 638284. JR acknowledges funding from the European Union's Horizon 2020 research and innovation programme under the Marie Sklodowska-Curie grant agreement No 786833.

References

[1] Ramírez J, *et al.* Variability of ventricular repolarization dispersion quantified by time-warping the morphology of the T-wave. IEEE TBME 2017;64(7):1619–30.

[2] Ramírez J, *et al.* T-wave morphology restitution predicts sudden cardiac death in patients with chronic heart failure. JAHA 2017;6(e005310):1–12.

[3] Madeiro JPV, *et al.* New approach for T-wave peak detection and T-wave end location in 12-lead paced ecg signals based on a mathematical model. Med Eng Physics 2013; 35(8):1105–15.

[4] García J, *et al.* Ecg-based detection of body position changes in ischemia monitoring. IEEE TMBE 2004;50(6):677–685.

[5] Palmieri F, *et al.* Monitoring blood potassium concentration in hemodialysis patients by quantifying T-wave morphology dynamics. Sci Rep 2021;11:Art. no. 3883.

[6] Palmieri F, *et al.* Potassium monitoring from multilead T-wave morphology changes during hemodyalisis: Periodic versus principal component analysis. CinC 2020;47:1–4.

[7] Recommendations for measurement standards in quantitative electrocardiography. Eur Heart J 1985;6(10):815–25.

[8] Martínez JP, *et al.* A wavelet-based ECG delineator: Evaluation on standard databases. IEEE TBME 2004;4(51):570–81.

[9] Meijborg VMF, *et al.* Electrocardiographic T wave and its relation with ventricular repolarization along major anatomical axes. Circ 2014;7:524—-531.

Address for correspondence:
Flavio Palmieri; Universitat Politècnica de Catalunya, Av. Diagonal 647, Barcelona 08028 Spain. flavio.palmieri@upc.edu